

# Predicting glioma histo-molecular diagnosis and prognosis: preoperative dynamic contrast-enhanced magnetic resonance imaging insights

Hui Ma\*, Shanmei Zeng\*, Yingqian Huang\*, Dingxiang Xie, Liwei Mazu, Nengjin Zhu, Jing Zhao, Zhiyun Yang, Jianping Chu

Department of Radiology, The First Affiliated Hospital, Sun Yat-sen University, Guangzhou, China

Contributions: (I) Conception and design: H Ma, S Zeng, Y Huang; (II) Administrative support: J Zhao, Z Yang, J Chu; (III) Provision of study materials or patients: J Zhao, Z Yang, J Chu; (IV) Collection and assembly of data: D Xie, L Mazu, N Zhu; (V) Data analysis and interpretation: H Ma, D Xie, L Mazu, N Zhu; (VI) Manuscript writing: All authors; (VII) Final approval of manuscript: All authors.

Correspondence to: Jianping Chu, MD, PhD; Zhiyun Yang, MD, PhD; Jing Zhao, MD, PhD. Department of Radiology, The First Affiliated Hospital, Sun Yat-sen University, No. 58 Zhongshan Er Road, Guangzhou 510080, China. Email: chujping@mail.sysu.edu.cn; yzhyun@mail.sysu.edu.cn; zhaoj23@mail.sysu.edu.cn.

**Background:** The preoperative prediction of glioma, integrated histological/molecular classification, and prognosis are critical for personalized patient management and treatment optimization. This study aimed to explore whether preoperative dynamic contrast-enhanced magnetic resonance imaging (DCE-MRI), an advanced MRI technique, can comprehensively and noninvasively evaluate gliomas.

**Methods:** Adult patients (June 2013 to May 2021) with diffuse glioma, retrospectively reclassified by the 2021 World Health Organization (WHO) classification criteria in this cohort study, underwent conventional and DCE-MRI examinations at our institution. Quantitative measurements, including the volume transfer constant (Ktrans), volume of extravascular extracellular space per unit volume of tissue (Ve), and rate constant of backflux (Kep), were derived from the tumor parenchyma areas. The diagnostic efficacy of glioma grading and genotyping, such as isocitrate dehydrogenase (*IDH*) and 1p/19q status, was evaluated using receiver operating characteristic (ROC) analysis. The prognostic predictive value was assessed using Cox or logistic regression analysis to build models visualized by nomograms. The area under the curve (AUC), calibration curves, and decision curves were used to evaluate the performance of these models.

**Results:** The study population consisted of 101 participants [mean age ± standard deviation (SD), 47.05±12.81 years (72 males and 29 females)]. Tumor.Kep.max emerged as the most crucial parameter, serving as an independent protective predictor of 1p/19q-codeletion [odds ratio (OR) and 95% confidence interval (CI): 0.98 (0.97–0.996), AUC: 0.71 (0.58–0.82)], whereas it was negatively associated with high-grade gliomas [OR: 0.972 (0.950–0.996), AUC: 0.87 (0.80–0.94)] and *IDH*-mutant [OR: 1.02 (1.000–1.03), AUC: 0.72 (0.61–0.81)]. Tumor.Ve.max demonstrated excellent diagnostic value [AUC: 0.93 (0.86–1.00); sensitivity, 100%; specificity, 90.7%; P<0.001] for diagnosing cyclin-dependent kinase inhibitor 2A/B (*CDKN2A/B*) status. Tumor Ktrans.max emerged as an independent prognostic risk factor for glioma patients [AUCs for 1-, 3-, and 5-year survival, 0.75 (0.58–0.92), 0.64 (0.47–0.82), and 0.66 (0.43–0.89), respectively].

**Conclusions:** DCE-MRI technology holds significant value in glioma diagnosis, particularly in integrated molecular diagnostics, predicting grading, molecular genotype including *IDH* status, and prognosis, thereby offering a comprehensive preoperative evaluation framework. This approach enables clinicians to accurately stratify patients, thus optimizing treatment strategies.

<sup>\*</sup>These authors contributed equally to this work as co-first authors.

**Keywords:** Glioma; magnetic resonance imaging (MRI); prognosis; genotype; grading

Submitted Jan 05, 2025. Accepted for publication Jul 10, 2025. Published online Sep 22, 2025. doi: 10.21037/qims-2025-36

View this article at: https://dx.doi.org/10.21037/qims-2025-36

## Introduction

Glioma heterogeneity significantly influences clinical treatment strategies and patient outcomes. Previous studies have highlighted that higher World Health Organization (WHO) classifications correlate with increased glioma malignancy and poorer prognosis. Additionally, the molecular profile of gliomas is crucial for diagnosis, surgery, and survival outcomes (1-3). However, traditional diagnosis has limitations, such as invasiveness, incomplete sampling, and an inability to fully capture tumor heterogeneity. Therefore, there is a pressing need for noninvasive methods to preoperatively predict glioma characteristics, WHO grade, molecular genetics, and survival.

Perfusion imaging, which visualizes tumor blood flow, microvasculature, and angiogenesis, has emerged as a promising noninvasive modality for glioma assessment (4,5). Dynamic contrast-enhanced (DCE) perfusion imaging, based on T1 signal changes, offers a detailed portrayal of the tumor microvasculature, including vessel density, blood-brain barrier (BBB) integrity, and permeability (6-8). Yan *et al.* demonstrated the superior performance of DCE magnetic resonance imaging (DCE-MRI) parameters in glioma grading and survival prediction compared with other imaging modalities, such as arterial spin labeling (ASL) or intravoxel incoherent motion (IVIM) diffusion-weighted imaging (DWI) (9). Thus, DCE-MRI plays a unique and irreplaceable role in preoperative glioma evaluation and warrants further investigation (10).

Numerous studies have underscored the utility of DCE-MRI in predicting tumor grade, survival, and specific molecular types, such as isocitrate dehydrogenase (*IDH*) mutations (11-14). However, gaps remain in understanding its full potential. Although studies have explored quantitative DCE-derived parameters, such as transfer constant (Ktrans), extracellular volume fraction (Ve), and reflux constant (Kep), less attention has been given to semiquantitative measures, such as the initial area under the curve (iAUC), which can provide insights into tumor physiology and blood volume variations (15). Additionally, there are limited data on how DCE-derived parameters correlate with molecular markers, such as cyclin-dependent kinase inhibitor 2A/B (*CDKN2A*/

B), chromosome 7 gain, and chromosome 10 loss (+7/-10), which are critical in glioma classification according to the 2021 WHO guidelines. Furthermore, some studies have suggested the use of histogram analysis to derive parameters such as mean and maximum values from regions of interest (ROI) for glioma assessment (16). This raises the question of whether the maximum, minimum, and average values from both the tumor parenchyma and peritumor parenchyma can effectively predict glioma diagnosis and prognosis.

Our study aimed to comprehensively explore and compare the preoperative utility of various DCE-MRI-derived parameters, including maximum, minimum, and average values from the tumor and peritumor parenchyma, in grading gliomas, identifying molecular subtypes, and predicting prognosis. Additionally, we constructed and presented predictive models in a nomogram format, offering a quantitative tool for individual risk prediction and patient benefit assessment. The evaluation of these nomograms will focus on their discrimination ability, accuracy, and clinical practicality to assess their overall clinical effectiveness. We present this article in accordance with the STROBE reporting checklist (available at https://qims.amegroups.com/article/view/10.21037/qims-2025-36/rc).

#### **Methods**

## Study participants

This study was conducted in accordance with the Declaration of Helsinki and its subsequent amendments. The study was approved by the Medical Ethics Committee of The First Affiliated Hospital of Sun Yat-sen University (No. [2021]209). The Ethics Committee waived the need for informed consent due to the retrospective nature of the study.

Patients [101 patients; mean age ± standard deviation (SD), 47.05±12.81 years; 72 males and 29 females] who underwent preoperative MRI at the First Affiliated Hospital of Sun Yatsen University (June 2013 to May 2021) and were confirmed to have adult-type diffuse gliomas by pathology were enrolled retrospectively. Additional inclusion and exclusion criteria are presented in *Figure 1*. Follow-up survival data were collected

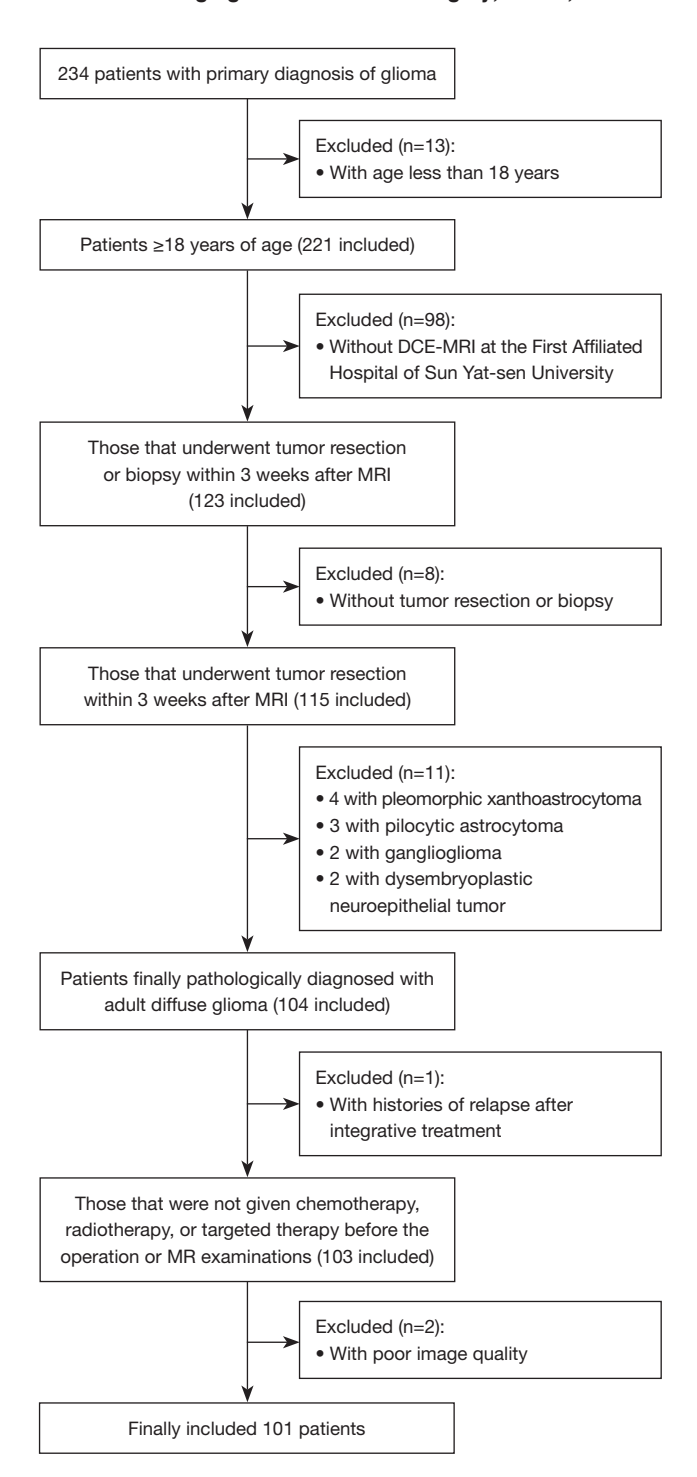


**Figure 1** Description of the inclusion and exclusion criteria. DCE, dynamic contrast-enhanced; MRI, magnetic resonance imaging.

through clinical interviews until 31 May 2021. Overall survival (OS) was defined as the duration from the date of primary tumor resection to the date of death, censored at the

date of the last follow-up visit if the patient was alive or lost to follow up.

# MRI protocol

Images were acquired using a 3.0T MR scanner (MAGNETOM Verio Prisma, Siemens Healthineers, Erlangen, Germany). The detailed imaging parameters are listed in *Table 1*. Each participant underwent conventional MRI sequences, including pre-contrast axial T1-weighted imaging (T1WI), axial T2-weighted imaging (T2WI), axial/coronal T2-fluid-attenuated inversion recovery (FLAIR) imaging, and axial T1-weighted contrast-enhanced imaging (T1CE), in addition to DCE-MRI.

The DCE-MRI protocol comprised two precontrast T1-volumetric interpolated breath-hold examination (T1-VIBE) sequences, each with distinct flip angles (2° and 15°), to calculate the T1-map, and dynamic contrast-enhanced time-resolved angiography with stochastic trajectories sequences (TWIST; 75 measurements, total scan time of 358 s). A bolus injection of 0.1 mmol/kg body weight of gadolinium (Magnevist, Schering, Berlin, Germany) at an injection rate of 4 mL/s was started from the fifth measurement of 75 phases in total, followed by a 20 mL 0.9% saline flush. Post-contrast sagittal three-dimensional (3D) T1-weighted magnetization-prepared rapid gradient-echo (MPRAGE) and T1CE images were obtained after DCE-MRI.

## DCE-MRI analysis

All DCE-MRI data were transmitted to a commercially available and clinically approved post-processing workstation (Sango via, Siemens Healthcare) for analysis using the Siemens Tissue 4D workflow according to the manufacturer's instructions. Automatic motion correction and alignment were first performed. The tissue signal intensity was converted to gadolinium concentration. The two-compartment Toft's model was used to fit the pharmacokinetic curves (17). Three types of the arterial input function (AIF; the slow, intermediate, and fast types), based on mathematical simulation, were automatically provided (18,19). According to the operation manual, one of the above three types with the smallest chi-square value was selected. ROIs were then sketched at the three consecutive and maximal levels of tumors after the consensus of two experienced radiologists according to previous studies (20-22). Within each level, two ROIs were positioned as follows:

Table 1 Parameters of MRI sequences

Parameters	T1WI	T2WI	T2-FLAIR	DCE	-MRI	T1-MPRAGE	T1CE
Parameters	Spin-echo	Turbo spin-echo	Turbo spin-echo	no T1-VIBE TWIST		Echo planar imaging	Spin-echo
Contrast agent	_	-	_	-	Gadolinium	Gadolinium	Gadolinium
Dose (mmol/Kg)	-	-	-	-		0.1	
Flip angles	150°	150°	150°	2°/15°	12°	8°	150°
TR/TE (ms/ms)	2,000/17	4,200/109	9,000/84	3.83/1.37	4.89/1.88	2,300/2.43	2,000/17
Slice thickness (mm)	6	6	6	3.5	3.5	0.75	6
Field of view (mm²)	220×220	220×220	220×220	220×220	220×220	240×225	220×220
Voxel resolution (mm³)	0.7×0.7×6	0.6×0.6×6	0.7×0.7×6	1.4×1.4×3.5	1.4×1.4×3.5	0.8×0.8×0.8	0.7×0.7×6

DCE-MRI, dynamic contrast-enhanced magnetic resonance imaging; MRI, magnetic resonance imaging; T1CE, T1-weighted contrast-enhanced imaging; T1-MPRAGE, T1-magnetization-prepared rapid gradient-echo; T1-VIBE, T1-volumetric interpolated breath-hold examination; T1WI, T1-weighted imaging; T2-FLAIR, T2-fluid-attenuated inversion recovery; T2WI, T2-weighted imaging; TE, echo time; TR, repetition time; TWIST, time-resolved angiography with stochastic trajectories sequences.

- ❖ One ROI (irregularly shaped) encompassed all solid components of the tumor parenchyma (hereinafter referred to as the "tumor" region), excluding large vessels, meninges, and necrotic and hemorrhagic areas. ROI placements on DCE-derived maps were performed using T1CE as the reference when tumors showed enhancement; if there was no enhancement, T2-FLAIR images were used as the reference to draw the ROIs.
- ❖ The other ROI (circular, measuring 10 mm²) was randomly placed on areas extending ≤1 cm from the tumor margin (expressed as "peritumoral" hereinafter).

Representative images of the ROIs are shown in *Figure 2*. Thus, quantitative parameters, including Ktrans, Ve, and Kep, and the semiquantitative parameter iAUC which was in the first 60 seconds, were calculated. The minimum, mean, and maximum values of each DCE-MRI metric in each layer were recorded, and the average values of the three levels of each metric were used for analysis. A total of 24 parameters [2 ROIs (tumor parenchyma/peritumoral) × 4 parameters (Ktrans/Kep/Ve/iAUC) per ROI × 3 statistical values (the average of the maximum/minimum/mean values across the three levels) per parameter] were derived, such as the minimum value of Ve derived from the tumor parenchyma (tumor.Ve.min).

#### Histopathological and molecular evaluation

The mutation statuses of *IDH1* and *IDH2* were determined using high-throughput sequencing methods. The status

of 1p/19q, epidermal growth factor receptor (*EGFR*), and *CDKN2A/B* was evaluated using fluorescence in situ hybridization (FISH) (23). Following the 2021 WHO Central Nervous System (CNS) classification, tumors were reclassified using an integrated histomolecular diagnosis, which incorporated existing molecular results and original pathologic diagnoses.

## Statistical analysis

The data were analyzed using the software SPSS 26 (IBM Corp., Armonk, NY, USA), the SPSSAU data scientific analysis platform (https://spssau.com/) (24), and the R programming language (version 4.1.2, The R Foundation for Statistical Computing, Vienna, Austria).

Normally distributed data are expressed as mean ± SD, and non-normally distributed data are expressed as median ± interquartile range (IQR). Univariate analysis was conducted using unpaired Student's *t*-tests, one-way analysis of variance (ANOVA), Mann-Whitney rank-sum tests, Kruskal-Wallis tests, or chi-square tests, if available. Multivariate analysis was performed using logistic or Cox regression models, incorporating age, sex, and univariate variables with a P value less than 0.1 as covariates. The predictive or prognostic models were comprehensively evaluated and compared using the area under the curve (AUC) calculated from receiver operating characteristic (ROC) curves and DeLong tests. Nomograms were constructed to visually represent these models using the R package nomogram and calibration curve analysis,

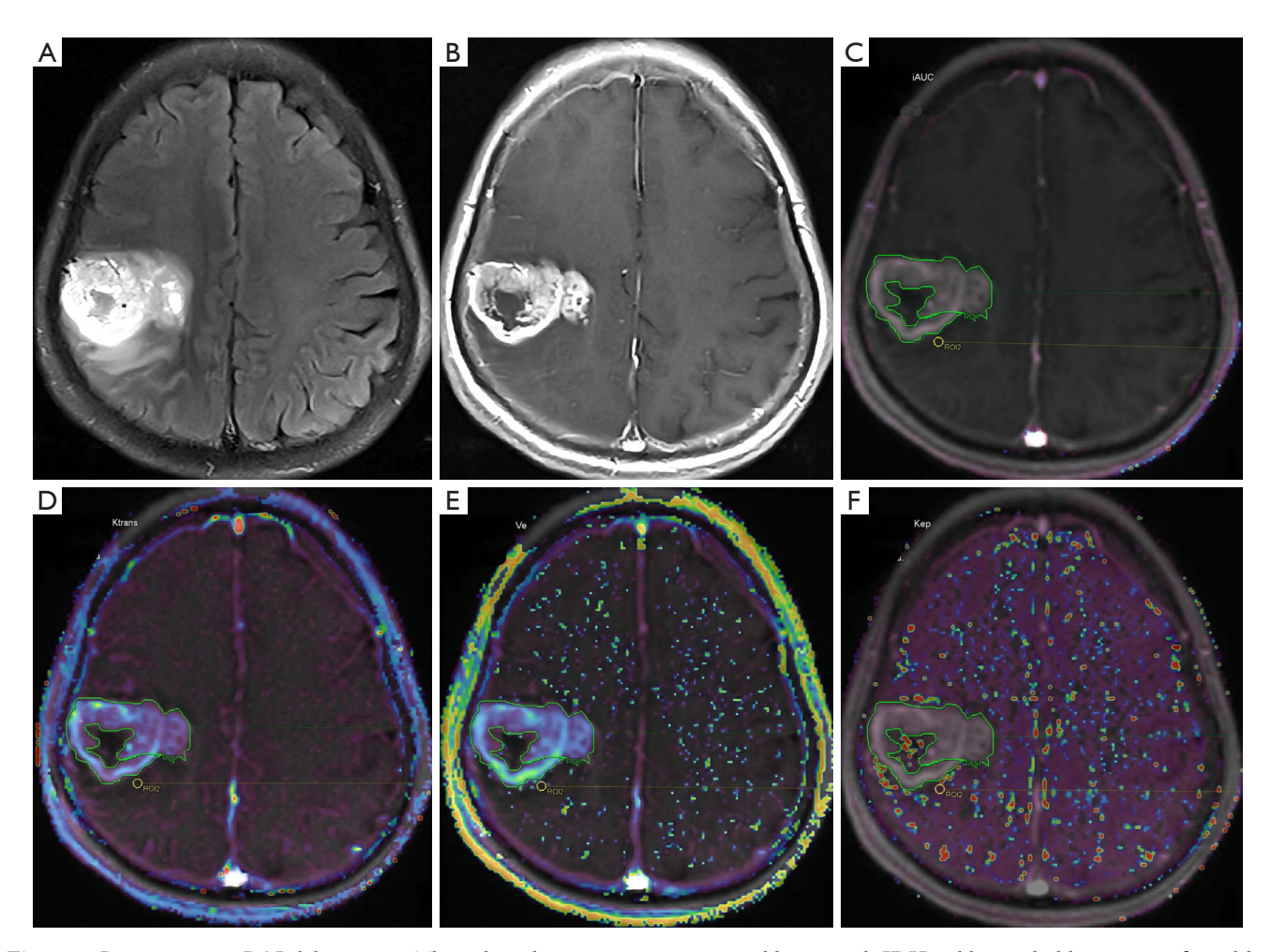


Figure 2 Representative ROI delineations. This selected patient was a 69-year-old man with IDH-wildtype glioblastoma confirmed by pathology. (A) T2-weighted FLAIR image; (B) contrast-enhanced T1-weighted image; (C) iAUC image; (D) Ktrans image; (E) Ve image; (F) Kep image. (C-F) ROI 1 (marked in green) represented the tumor parenchyma tissues, and ROI 2 (marked in yellow) represented the peripheral zones. FLAIR, fluid-attenuated inversion recovery; *IDH*, isocitrate dehydrogenase; iAUC, initial area under the curve for the first 60 seconds; ROI, region of interest.

and decision curve analysis (DCA) was performed (25). Furthermore, the 1-, 2-, and 5-year survival rates of individuals were predicted. Statistical significance was set at P<0.05, and the results were presented with a 95% confidence interval (CI) in parentheses.

### **Results**

# Demographic and oncological information

Patient demographic information and oncological characteristics, including histopathological and molecular data, are presented in *Table 2*. There were 61/101 high-

grade gliomas (HGGs; WHO grade 4) and 40/101 low-grade gliomas (LGGs; WHO grade 2 and 3). Notably, 23 individuals harbored *IDH*-mutant astrocytoma (12 classified as WHO grade 2, 5 as grade 3, and 6 as grade 4), 14 presented with *IDH*-mutant and 1p/19q-codeleted oligodendroglioma (11 cases of WHO grade 2 and 3 of grade 3), and 55 had grade 4 *IDH*-wildtype glioblastoma, according to the WHO 2021 classification. A total of 9 cases were classified as *IDH*-wildtype, not otherwise specified (NOS), because of incomplete information, and the detailed molecular information is shown in Table S1. Until 31 May 2021, 49 (48.5%) patients were alive, 41 (40.6%) had died,

Table 2 Participant demographic, histopathologic, and molecular data

Barrandar	Mondo		Gender (n=101)		Age (years)		
Parameter	Number	Male (n=72)	Female (n=29)	P value	Mean ± SD	P value	
Group	101			0.82		<0.0001****	
Low-grade	40	28	12		39.80±9.50		
High-grade	61	44	17		51.80±12.52		
CNS WHO grade	101			0.84		<0.0001****	
Grade 2	29	21	8		39.27±9.32		
Grade 3	11	7	4		41.40±10.36		
Grade 4	61	44	17		51.80±12.52		
IDH	101			0.78		<0.0001****	
Wild-type	64	45	19		52.38±11.83		
Mutant	37	27	10		37.84±8.56		
1p/19q	85			0.25		0.01*	
Codeletion	19	16	3		40.63±9.17		
Non-codeletion	66	47	19		47.70±13.22		
EGFR amplification	56			0.95		0.31	
No amplification	37	25	12		50.97±13.85		
Amplification	19	13	6		54.63±9.33		
+7/-10 cytogenetic signature	20			0.52		0.06	
No +7/-10	18	11	7		42.50±13.19		
+7/–10	2	2	0		62.00±11.31		
CDKN2A/B homozygous deletion	48			0.94		0.13	
No deletion	43	35	8		40.16±11.14		
Deletion	5	4	1		48.40±11.74		
Integrated histomolecular diagnosis	101			0.40		<0.0001****	
Astrocytoma, IDH-mutant	23	14	7		36.65±7.52		
Oligodendroglioma, <i>IDH</i> -mutant and 1p/19q codeleted	14	12	2		39.79±10.03		
Glioblastoma, IDH-wildtype	55	35	13		53.45±11.87		
IDH-wildtype, NOS	9	5	4		45.78±9.73		

<sup>\*,</sup> P<0.05; \*\*\*\*, P<0.0001. CDKN2A/B, cyclin-dependent kinase inhibitor 2A/B; CNS, central nervous system; *EGFR*, epidermal growth factor receptor; *IDH*, isocitrate dehydrogenase; NOS, not otherwise specified; SD, standard deviation; WHO, World Health Organization.

and 11 (10.9%) had been lost to follow-up.

As shown in *Table 2*, only age but not sex was found to be significantly associated with genotype, such as *IDH* and 1p/19q status, diagnosis, and tumor grade. Specifically, gliomas with high-grade, *IDH*-wildtype, and 1p/19q-noncodeletion tended to occur in older patients.

# Glioma grading with DCE-MRI-related parameters

# Different groups of HGG and LGG

According to the univariate analysis (Table S2), parameters derived from the tumor parenchyma, including the maximum, mean, and minimum values, significantly

differentiated LGGs from HGGs (P<0.05). Specifically, Kep values were lower in HGGs, whereas other parameters exhibited higher values in HGGs. Furthermore, the tumor. iAUC.mean significantly demonstrated the highest AUC [0.853 (0.763–0.920)] with the best 90.2% sensitivity and 70% specificity using the optimal-retrospectively determined threshold of 0.08 (P<0.05, Table S2 and Figure 3A).

Subsequently, multivariate logistic regression analysis revealed that age [odds ratio (OR): 1.058 (1.007–1.110)] and tumor.Kep.max [OR: 0.972 (0.950–0.996)] were promoting factors for predicting HGGs (P<0.05, *Table 3*). However, compared to univariate analysis using tumor. iAUC.mean, the prediction model did not exhibit improved discrimination ability with a greater AUC [0.87 (0.80–0.94), P>0.05, *Figure 3A*].

The model was visualized using a nomogram (*Figure 3B*) with good diagnostic capability and adequate calibration (*Figure 3C*). DCA (*Figure 3D*) further confirmed the clinical validity of the model, revealing that the cutoff value of 0.54 determined by ROC analysis fell within the range of threshold probabilities (0.03–0.78).

# Subgroup analysis of WHO Grades 2, 3, and 4

The univariate analysis revealed that parameters derived from the tumor parenchyma, peritumoral-iAUC-max, and peritumoral-iAUC-mean could differentiate different grades of gliomas (P<0.05, Table S3). However post hoc pairwise comparisons showed that only parameters derived from the tumor parenchyma effectively differentiated gliomas with WHO grades 2 and 4 (P<0.001), or between WHO grades 2 and 3 (P<0.05); meanwhile, no statistically significant differences were observed between grades 3 and 4 (Table S3).

Multivariate logistic regression analysis (*Table 3*) revealed that WHO grade exhibited a positive correlation with age [OR: 1.068 (1.004–1.136)] and a negative correlation with tumor.Kep.max [OR: 0.973 (0.95–0.997)]. The prediction model successfully discriminated gliomas with WHO grades of 2 [AUC, 0.893 (0.815–0.957), *Figure 3E* and Table S4] and 4 [AUC, 0.858 (0.776–0.931), *Figure 3F* and Table S5].

Furthermore, the models were visualized using nomograms (*Figure 3G*, *3H*) with strong diagnostic capability and adequate calibration (*Figure 3I*, *3f*). DCA (*Figure 3K*, *3L*) further confirmed the wide clinical validity of the model within the range of threshold probabilities (0.05–0.89 or 0.05–0.81).

## Glioma genotyping with DCE-MRI-related parameters

## IDH gene

According to the univariate analysis (Table S6), the results were comparable to those observed in the above groups. Specifically, in predicting *IDH* genotype, tumor.iAUC.mean performed the best [AUC, 0.770 (0.690–0.868), *Figure 4A*], with the best specificity of 86.5%, although there was no evidence of a difference compared to the others (P>0.05).

According to the multivariate analysis (*Table 3*), tumor. Kep.max was independently associated with *IDH* status [OR: 1.015 (1.000–1.029)], and age was negatively associated with survival [OR: 0.894 (0.851–0.939)]. Compared to the highest AUC in the univariate analysis, the predictive power of this multifactor model [AUC, 0.855 (0.779–0.920)] improved significantly (P<0.05). Furthermore, this predictive model was visualized using a nomogram (*Figure 4B*) with good diagnostic capability, adequate calibration ability, and wide clinical validity within the range of threshold probabilities (0.06–0.84) (*Figure 4C,4D*).

## 1p/19q

The univariate analysis (Table S7) revealed that Ktrans. min had the best specificity for predicting 1p/19q in tumors (84.2%), and Kep.max exhibited the best sensitivity (73.7%). Furthermore, Kep.mean demonstrated the highest AUC [0.708 (0.563–0.835), *Figure 4E*].

According to the logistic regression analysis (*Table 3*), tumor.Kep.max served as an independent predictive factor for 1p/19q codeletion [OR: 0.982 (0.968–0.996)]. However, the predictive power of this model did not improve [AUC, 0.705 (0.581–0.821), P<0.05].

Nomograms were constructed (*Figure 4F*), and DCA indicated the acceptable potential clinical usefulness of the nomograms (*Figure 4G*). Nevertheless, the calibration plot revealed a deviation from the true events, suggesting that the model was not well calibrated (*Figure 4H*).

## CDKN2A/B gene

In diagnosing the *CDKN2A/B* genotype, Ve, Kep, and iAUC obtained from the tumor parenchyma provided excellent diagnostic values (*Figure 4I* and Table S8, P<0.01). Remarkably, tumor.Ve.max achieved the largest AUC of 0.93, coupled with 100% sensitivity and 90.7% specificity, using an optimal retrospectively determined threshold of 2.87. Additionally, Kep showed 100% specificity and was lower for tumors with homozygous CDKN2A/B deletion

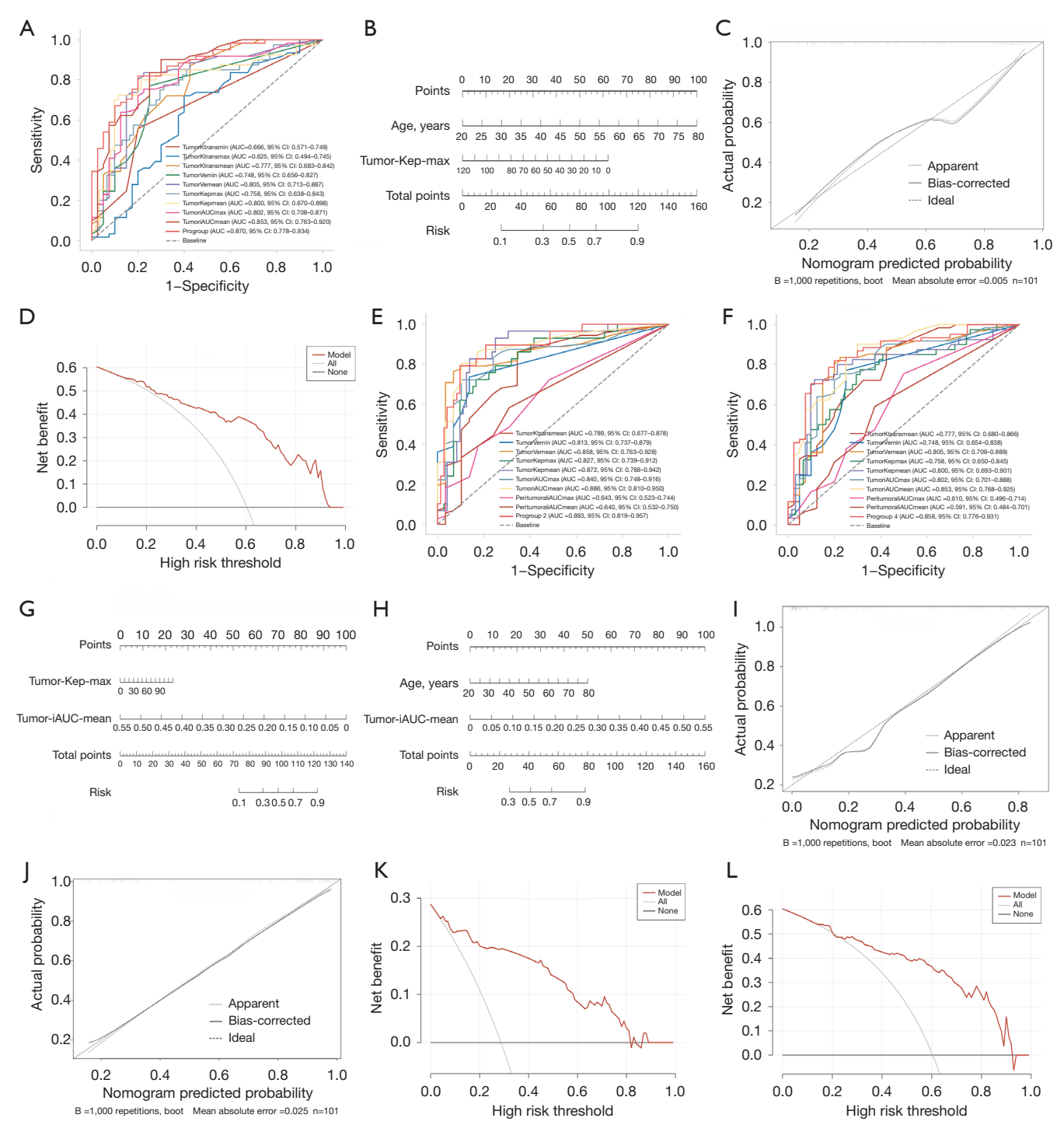


Figure 3 ROC curve plots with AUCs of all selective DCE-MRI-related parameters and corresponding predictive models for differentiating LGGs and HGGs (A), WHO grade 2 (E), and WHO grade 4 (F) gliomas. Nomograms for individually predicting the probability of high-grade (B), WHO grade 2 (G), and WHO grade 4 (H) gliomas. Calibration plots of corresponding predictive models for differentiating LGGs and HGGs (C), WHO grade 2 (I), and WHO grade 4 (J) gliomas. DCAs of corresponding predictive models for differentiating LGGs and HGGs (D), WHO grade 2 (K), and WHO grade 4 (L) gliomas. AUC, area under the curve; DCA, decision curve analysis; DCE-MRI, dynamic contrast-enhanced magnetic resonance imaging; HGGs, high-grade gliomas; iAUC, initial area under the curve for the first 60 seconds; LGGs, low-grade gliomas; ROC, receiver operating characteristic; WHO, World Health Organization.

P (for HL) **Predictors** Parameter β SE P (for β) OR (95% CI) 0.06 0.03 0.02\* 1.058 (1.007-1.110) Group Age 0.69 tumor.Kep.max -0.030.01 0.02\* 0.972 (0.950-0.996) Grade 0.26 0.07 0.03 0.04\* 1.07 (1.004-1.14) Age tumor.Kep.max 0.973 (0.95-0.997) -0.030.01 0.03\* IDH Aae 0.15 -0.110.03 < 0.001\*\*\* 0.89 (0.85-0.94) tumor.Kep.max 0.01 0.01 0.049\* 1.02 (1.00-1.03) Constant 3.81 1.18 0.01\* 47.78 (4.46-511.67) tumor.Kep.max 0.982 (0.968-0.996) 1p/19q 0.03 -0.020.01 0.01\* <0.001\*\*\* 2.14 0.49 8.50 (3.28-22.02) Constant CDKN2A/B tumor.Ve.max 0.001 13.19 8.77 0.13 5.36×10<sup>5</sup> (0.019-1.55×10<sup>13</sup>)

Table 3 The logistic regression results for predicting gliomas of different group (HGG or LGG), different WHO grade, IDH-mutant, 1p/19q codeletion, CDKN2A/B homozygous deletion

25.82

0.13

-39.3

than for those without CDKN2A/B deletion.

Constant

Unfortunately, despite these promising results, no significant variables were incorporated into the logistic regression equation to predict the *CDKN2A/B* status. Furthermore, the model was visualized using nomograms (*Figure 4f*), which exhibited good diagnostic capability; however, the calibration plot revealed a deviation from true events, suggesting that the model was not well calibrated (*Figure 4K*). DCA (*Figure 4L*) revealed that the model demonstrated an acceptable clinical validity.

### EGFR and +7/-10 cytogenetic signature

To determine the *EGFR* or +7/-10 type (Tables S9,S10), Ve derived from the peritumoral area had the smallest P value of 0.061 and 0.058 (borderline significant, respectively). ROC analysis revealed that the AUC was 0.649 or 0.917 (P=0.069 or 0.059), with 73.7% or 100% specificity and 59.5% or 83.3% sensitivity for predicting EGFR amplification or the +7/-10 cytogenetic signature, respectively. However, they did not establish a related prediction model.

### Glioma prognosis with DCE-MRI-related parameters

The final multivariate Cox regression analysis identified tumor.Ktrans.max [HR: 1.70 (1.05–2.74)], and tumor.

iAUC.min [HR: 4.34 (1.60–11.79)] as independent prognostic risk factors for glioma patients (P<0.05, *Table 4*). Time-dependent ROC analysis revealed AUC values with 95% CI of 0.75 (0.58–0.92), 0.64 (0.47–0.82), and 0.66 (0.43–0.89) for 1-, 3-, and 5-year survival, respectively (*Figure 5A*). Adequate calibration (*Figure 5B*) was developed for practical use, and a nomogram (*Figure 5C*) exhibited acceptable stratification capacity. The DCAs (*Figure 5D-5F*) demonstrated that the prognostic model offered a good overall net benefit for 1-year survival outcome (*Figure 5D*), indicating its strong potential for predicting the survival of patients with glioma.

0 (0-8.21×10<sup>5</sup>)

#### **Discussion**

Based on the latest 2021 WHO classification, this retrospective study aimed to investigate the clinical utility of preoperative DCE-derived parameters in adult diffuse gliomas. Our findings indicate that certain DCE-derived parameters, such as the maximum values of Kep and Ktrans derived from tumor tissue, exhibit excellent diagnostic performance in predicting glioma prognosis and grading, as well as identifying the genetic status of *IDH*, 1p/19q, and *CDKN2A/B* (Table S11). Additionally, we provided diagnostic threshold values for various significant parameters and visualized prediction models

<sup>\*,</sup> P<0.05; \*\*\*, P<0.001. β, regression coefficient; CDKN2A/B, cyclin-dependent kinase inhibitor 2A/B; CI, confidence interval; HGG, high-grade glioma; HL, Hosmer-Lemeshow test; IDH, isocitrate dehydrogenase; LGG, low-grade glioma; OR, odds ratio; SE, standard error of regression coefficient; WHO, World Health Organization.

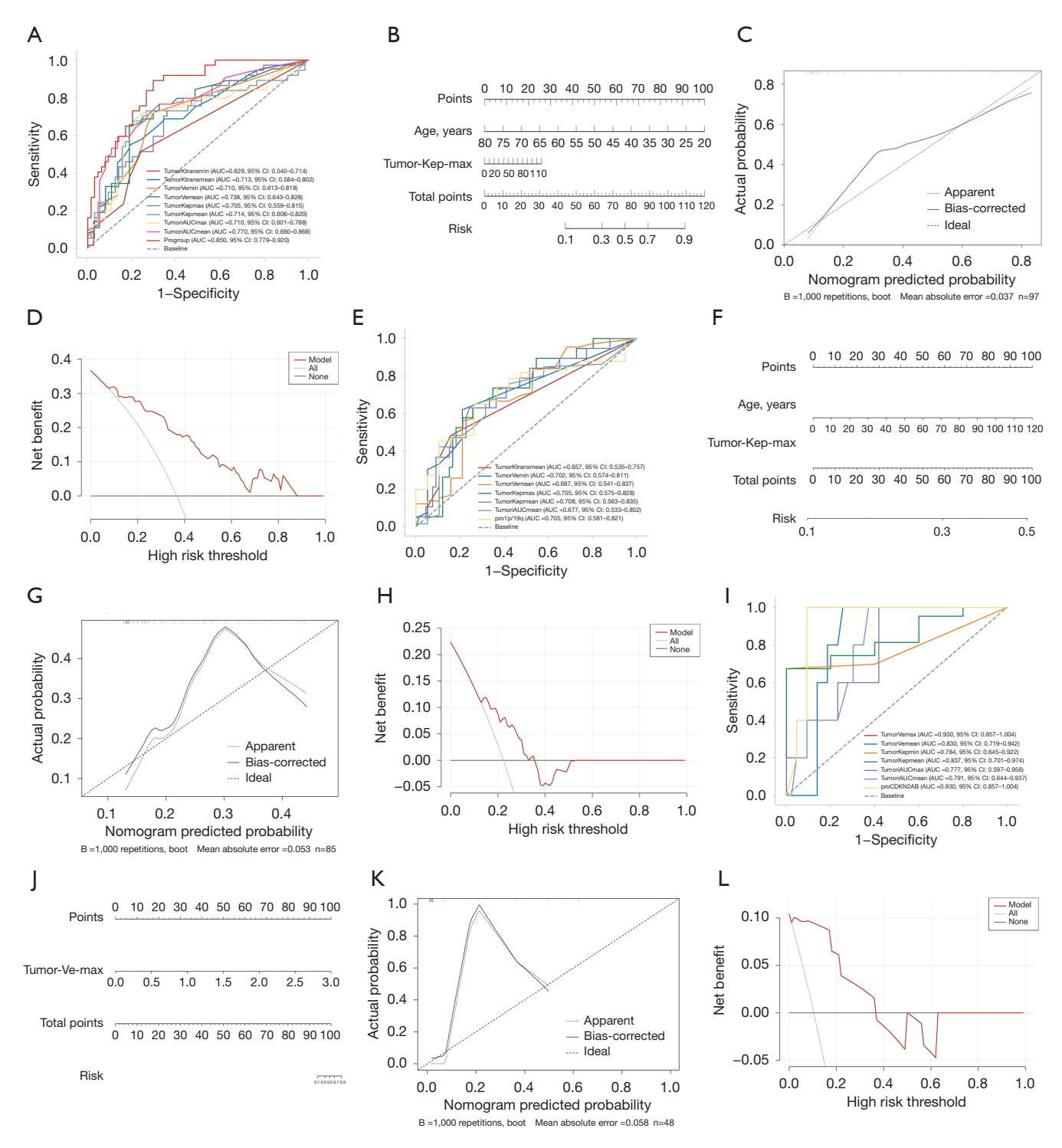


Figure 4 ROC curve plots with AUCs of all selective DCE-MRI-related parameters and corresponding predictive models, calibration plots, and DCAs of corresponding predictive models for differentiating different *IDH* genotypes (A,C,D), different 1p/19q genotypes (E,G,H), and different *CDKN2A/B* genotypes (I,K,L). Nomograms for individually predicting the probability of *IDH* mutation (B), 1p/19q codeletion (F), and *CDKN2A/B* homozygous deletion (J) gliomas. AUC, area under the curve; CDKN2A/B, cyclin-dependent kinase inhibitor 2A/B; DCA, decision curve analysis; DCE-MRI, dynamic contrast-enhanced magnetic resonance imaging; iAUC, initial area under the curve for the first 60 seconds; *IDH*, isocitrate dehydrogenase; ROC, receiver operating characteristic.

Table 4 The results of Cox regression

Mariana	Univaria	ate Cox regression	Multivariate Cox regression							
Variance	Р	HR (95% CI)	β	SE	Р	HR (95% CI)				
Age	_	-	-	_	ns	-				
Sex	_	-	-	-	ns	-				
tumor.Ktrans.max	0.03*	1.27 (1.03–1.56)	0.53	0.24	0.03*	1.70 (1.05–2.74)				
tumor.Ktrans.mean	0.06	5.67 (0.96–33.35)	-	-	ns	-				
peritumoral.Ve.max	0.08	1.599 (0.95–2.69)	-	-	ns	-				
peritumoral.Ve.mean	0.01*	6.03 (1.58–22.99)	-	-	ns	-				
tumor.iAUC.min <sup>†</sup>	0.001**	3.54 (1.67–7.50)	1.47	0.51	0.004**	4.34 (1.60–11.79)				

 $<sup>^{\</sup>dagger}$ , this continuous variable was transformed into categorical variables according to the mode "0". ns, P>0.05; \*, P<0.05; \*\*, P<0.01.  $\beta$ , regression coefficient; CI, confidence interval; HR, hazard ratio; iAUC, initial area under the curve for the first 60 seconds; SE, standard error of regression coefficient.

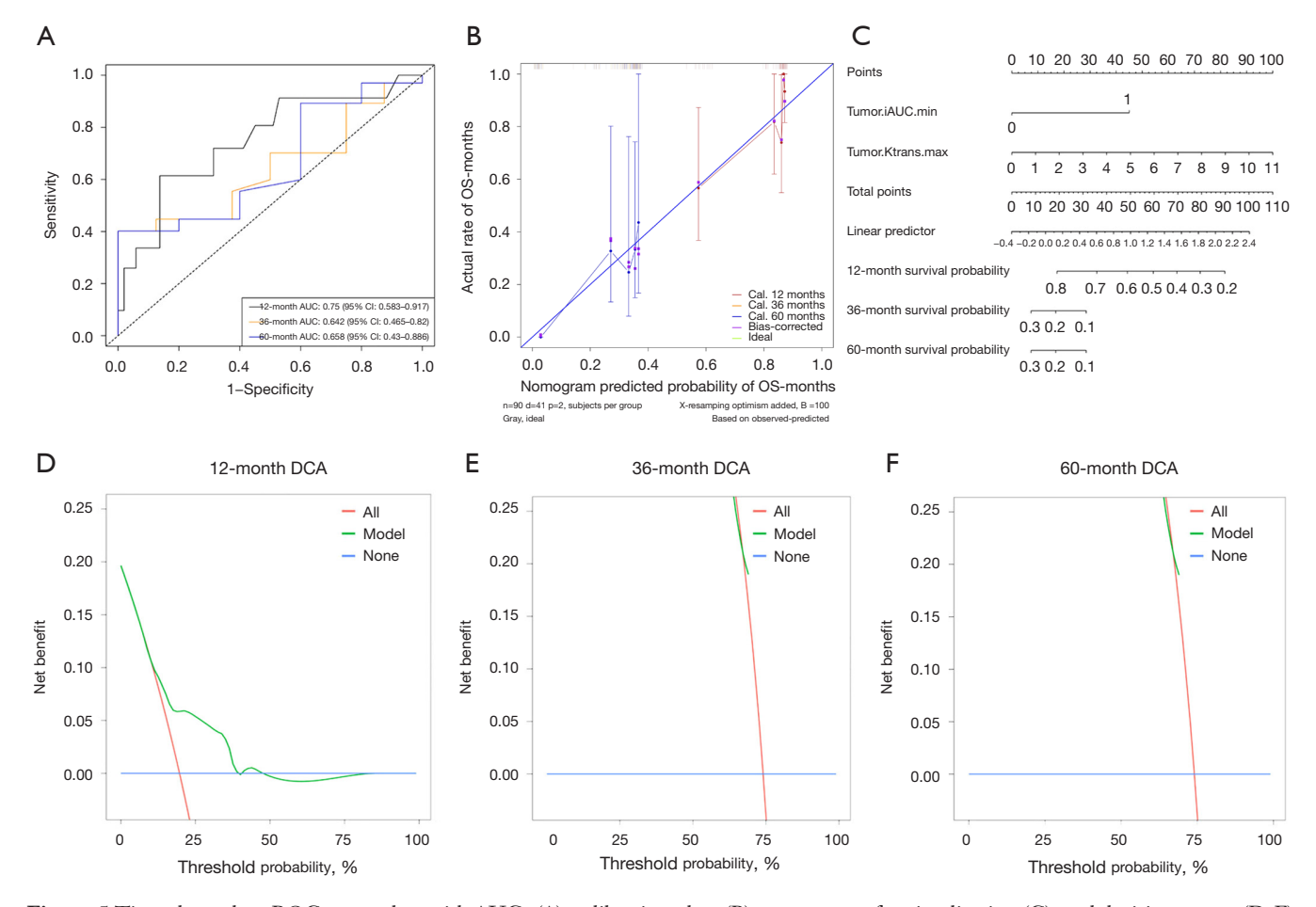


Figure 5 Time-dependent ROC curve plots with AUCs (A), calibration plots (B), nomograms for visualization (C), and decision curves (D-F) of the Cox regression model for 1-, 3-, and 5-year overall survival with all selected DCE-MRI-related parameters. AUC, area under the curve; DCA, decision curve analysis; DCE-MRI, dynamic contrast-enhanced magnetic resonance imaging; iAUC, initial area under the curve for the first 60 seconds; OS, overall survival; ROC, receiver operating characteristic.

using nomograms, which offer a relatively quantitative and intuitive approach with clinically useful thresholds to meet the practical needs of clinical decision-makers.

According to the univariate analysis, numerous DCErelated parameters were significantly different between HGGs and LGGs, between WHO grade 2- and 3gliomas, between WHO grade 2- and 4- gliomas, and between different statuses of IDH, 1p/19q, and CDKN2A/ B, as well as for predicting glioma prognosis. Notably, tumor.Kep.max emerged as the most crucial parameter because it served as an independent predictive factor in several final prediction models. Kep is known to reflect vessel permeability and surface area (26). More malignant and infiltrative gliomas are associated with increased permeability and larger surface areas, leading to the accumulation of contrast agents in the extravascular compartment, resulting in delayed reverse transfer and a decreased rate (27). Accordingly, lower Kep values indicate higher glioma grades and IDH-wild genotypes (27). Possible reasons for these findings include variations in grouping criteria (some studies classify HGG as WHO grades 3 and 4), differences in the WHO CNS edition, and patient cohorts. Another explanation is that our study utilized genomic sequence analysis to detect both IDH1 and IDH2 mutations, whereas previous studies primarily focused on IDH1 R132H mutation detection using immunohistochemistry, which represents only the most common mutation in gliomas (5,28-30). This approach may have resulted in slightly higher false-negative rates, such as missing mutations in IDH2 (27).

Regarding 1p/19q status, Santwijk *et al.* concluded that the impact of 1p/19q codeletion on DCE-related metrics remains poorly understood and has not been fully elucidated despite a systematic literature search (5). In addition, Ahn *et al.* demonstrated that DCE indices were not significantly associated with 1p/19q codeletion in LGG (28). However, in our study, a lower Kep tended to be 1p/19q-codeleted. Therefore, our findings provide valuable insights into this field of research.

To the best of our knowledge, there are limited studies predicting *CDKN2A/B* or +7/-10 status using MR, particularly DCE-MRI (14,31-36). Importantly, our study revealed that Ve derived from tumor tissue is an independent positive predictor of *CDKN2A/B* status. We hypothesized that this may be due to the correlation between Ve and cellularity/mitotic activity (37,38). Although our study was one of the earlier studies to attempt to predict the +7/-10 status using DCE-derived parameters,

the results were not promising. Nevertheless, our data provide preliminary evidence of a correlation between DCE-derived parameters and *CDKN2A/B* phenotypes.

Contrary to our expectations, no significant parameters were associated with *EGFR* amplification, which plays a crucial role in promoting tumor growth and invasion. We speculate that this may be attributed to an unbalanced patient population and insufficient sample size, which may have led to selection bias and limited the power of the analysis to detect differences in DCE-derived indices. Future studies with larger sample sizes and additional genetic testing are required to resolve this uncertainty.

Consistent with the established literature, our study reaffirmed the prognostic value of Ktrans and iAUC derived from tumor, demonstrating that higher Ktrans was associated with worse OS or higher HR, and the iAUC was found to be an independent negative prognostic factor (39-41). Notably, our analysis revealed diminished prognostic utility of peritumoral DCE-MRI parameters for molecular marker prediction and survival outcome assessment—a finding that diverges from prior HGGspecific studies reporting improved OS associated with high Ve in peritumoral edema (26). This discrepancy may be multifactorial. Primarily, the inclusion of LGG cases in our cohort introduced distinct pathophysiological characteristics, particularly relatively restricted peritumoral infiltration compared to the HGG populations examined in previous investigations. Furthermore, technical limitations warrant consideration, including (I) intrinsic heterogeneity within the peritumoral microenvironment affecting parameter consistency; and (II) non-standardized ROI selection protocols in peritumoral regions. In future studies, we plan to prioritize areas with higher tumor infiltration for ROI placement, although accurately identifying such regions remains a methodological challenge.

This study has some limitations. First, despite exceeding the numbers of patients in many previous studies (4,27,29,42,43), the sample size remains limited. Second, the data were retrospectively collected from a single center, potentially introducing selection bias. Third, owing to technical constraints, this study did not analyze the prognostic marker *TERT* or another DCE-derived parameter, Vp. Future investigations that incorporate more molecular markers, integrated histopathological verification, and expanded measurements of Vp through multicenter retrospective or prospective studies are warranted to provide more insightful results regarding the clinical applications of DCE-MRI.

#### **Conclusions**

This study comprehensively evaluated the performance of DCE-derived parameters in patients with glioma, highlighting the clinical value of DCE-MRI in the diagnosis of glioma, especially for integrated molecular diagnostics and prognosis. We also developed convenient and effective prediction models and nomograms for use by clinicians. Future studies with larger sample sizes, such as those for *TERT*, *EGFR*, and +7/–10, will further refine the predictive ability of DCE-MRI for genotyping performance.

## **Acknowledgments**

We sincerely thank Prof. Shen Guoping for his valuable guidance and support in the survival analysis components of this study. His expertise was instrumental in this aspect of the research, and we acknowledge this contribution with appreciation.

## **Footnote**

Reporting Checklist: The authors have completed the STROBE reporting checklist. Available at https://qims.amegroups.com/article/view/10.21037/qims-2025-36/rc

Data Sharing Statement: Available at https://qims.amegroups.com/article/view/10.21037/qims-2025-36/dss

Funding: This work was supported by the National Natural Science Foundation of China (Nos. 82172015, 82202217, and 82402232), Guangdong Basic and Applied Basic Research Foundation (Nos. 2024A1515030233, 2024A1515013041 and 2025A1515012827), the Science and Technology Program of Guangzhou, China (No. 202201011244), Beijing Xisike Clinical Oncology Research Foundation (No. Y-zai2022/qn-0250), and National Innovation Center For Advanced Medical Devices (No. NMED2024CX-03-004).

Conflicts of Interest: All authors have completed the ICMJE uniform disclosure form (available at https://qims.amegroups.com/article/view/10.21037/qims-2025-36/coif). The authors have no conflicts of interest to declare.

Ethical Statement: The authors are accountable for all aspects of the work in ensuring that questions related to the accuracy or integrity of any part of the work are

appropriately investigated and resolved. This study was conducted in accordance with the Declaration of Helsinki and its subsequent amendments. The study was approved by the Medical Ethics Committee of The First Affiliated Hospital of Sun Yat-sen University (No. [2021]209). The Ethics Committee waived the need for informed consent due to the retrospective nature of the study.

Open Access Statement: This is an Open Access article distributed in accordance with the Creative Commons Attribution-NonCommercial-NoDerivs 4.0 International License (CC BY-NC-ND 4.0), which permits the noncommercial replication and distribution of the article with the strict proviso that no changes or edits are made and the original work is properly cited (including links to both the formal publication through the relevant DOI and the license). See: https://creativecommons.org/licenses/by-nc-nd/4.0/.

#### **References**

- Ostrom QT, Cioffi G, Waite K, Kruchko C, Barnholtz-Sloan JS. CBTRUS Statistical Report: Primary Brain and Other Central Nervous System Tumors Diagnosed in the United States in 2014-2018. Neuro Oncol 2021;23:iii1-iii105.
- 2. Weller M, van den Bent M, Preusser M, Le Rhun E, Tonn JC, Minniti G, et al. EANO guidelines on the diagnosis and treatment of diffuse gliomas of adulthood. Nat Rev Clin Oncol 2021;18:170-86.
- 3. Wen PY, Packer RJ. The 2021 WHO Classification of Tumors of the Central Nervous System: clinical implications. Neuro Oncol 2021;23:1215-7.
- Hilario A, Hernandez-Lain A, Sepulveda JM, Lagares A, Perez-Nuñez A, Ramos A. Perfusion MRI grading diffuse gliomas: Impact of permeability parameters on molecular biomarkers and survival. Neurocirugia (Engl Ed) 2019;30:11-8.
- van Santwijk L, Kouwenberg V, Meijer F, Smits M,
  Henssen D. A systematic review and meta-analysis on
  the differentiation of glioma grade and mutational status
  by use of perfusion-based magnetic resonance imaging.
  Insights Imaging 2022;13:102.
- 6. Chung H, Seo H, Choi SH, Park CK, Kim TM, Park SH, Won JK, Lee JH, Lee ST, Lee JY, Hwang I, Kang KM, Yun TJ. Cluster Analysis of DSC MRI, Dynamic Contrast-Enhanced MRI, and DWI Parameters Associated with Prognosis in Patients with Glioblastoma after Removal

- of the Contrast-Enhancing Component: A Preliminary Study. AJNR Am J Neuroradiol 2022;43:1559-66.
- Park YW, Ahn SS, Moon JH, Kim EH, Kang SG, Chang JH, Kim SH, Lee SK. Dynamic contrast-enhanced MRI may be helpful to predict response and prognosis after bevacizumab treatment in patients with recurrent highgrade glioma: comparison with diffusion tensor and dynamic susceptibility contrast imaging. Neuroradiology 2021;63:1811-22.
- Guida L, Stumpo V, Bellomo J, van Niftrik CHB, Sebök M, Berhouma M, Bink A, Weller M, Kulcsar Z, Regli L, Fierstra J. Hemodynamic Imaging in Cerebral Diffuse Glioma-Part A: Concept, Differential Diagnosis and Tumor Grading. Cancers (Basel) 2022.
- Yan LF, Sun YZ, Zhao SS, Hu YC, Han Y, Li G, Zhang X, Tian Q, Liu ZC, Yang Y, Nan HY, Yu Y, Sun Q, Zhang J, Chen P, Hu B, Li F, Han TH, Wang W, Cui GB. Perfusion, Diffusion, Or Brain Tumor Barrier Integrity: Which Represents The Glioma Features Best? Cancer Manag Res 2019;11:9989–10000.
- Zhou J, Hou Z, Tian C, Zhu Z, Ye M, Chen S, Yang H, Zhang X, Zhang B. Review of tracer kinetic models in evaluation of gliomas using dynamic contrast-enhanced imaging. Front Oncol 2024;14:1380793.
- 11. Zhou J, Duan S, Zhu Z, Wang H, Tian C, Yang H, Chen S, Ye M, Zhang X, Zhang B. Identification of intrinsic imaging subtypes using clustering analysis based on dynamic contrast-enhanced magnetic resonance imaging radiomics features for gliomas: preliminary associations with gene expression profiles. Quant Imaging Med Surg 2025;15:4734-47.
- 12. Ye M, Cao Z, Zhu Z, Chen S, Zhou J, Yang H, Li X, Chen Q, Luan W, Li M, Tian C, Sun T, Shi F, Zhang X, Zhang B. Integrating quantitative DCE-MRI parameters and radiomic features for improved IDH mutation prediction in gliomas. Front Oncol 2025;15:1530144.
- 13. Zhao K, Huang H, Gao E, Qi J, Chen T, Zhao G, Zhao G, Zhang Y, Wang P, Bai J, Zhang Y, Hou Z, Cheng J, Ma X. Distributed parameter model of dynamic contrastenhanced MRI in the identification of IDH mutation, 1p19q codeletion, and tumor cell proliferation in glioma patients. Front Oncol 2024;14:1333798.
- 14. Yang H, Zhu Z, Long C, Niu F, Zhou J, Chen S, Ye M, Peng S, Zhang X, Chen Y, Wei L, Wang H, Liu D, Yao M, Zhang X, Zhang B. Quantitative and Qualitative Parameters of DCE-MRI Predict CDKN2A/ B Homozygous Deletion in Gliomas. Acad Radiol 2024;31:3355-65.

- 15. Jing H, Yan X, Li J, Qin D, Zhang N, Zhang H. The Value of Dynamic Contrast-Enhanced Magnetic Resonance Imaging (DCE-MRI) in the Differentiation of Pseudoprogression and Recurrence of Intracranial Gliomas. Contrast Media Mol Imaging 2022;2022:5680522.
- Arevalo-Perez J, Peck KK, Young RJ, Holodny AI, Karimi S, Lyo JK. Dynamic Contrast-Enhanced Perfusion MRI and Diffusion-Weighted Imaging in Grading of Gliomas. J Neuroimaging 2015;25:792-8.
- Roniotis A, Oraiopoulou ME, Tzamali E, Kontopodis E, Van Cauter S, Sakkalis V, Marias K. A Proposed Paradigm Shift in Initializing Cancer Predictive Models with DCE-MRI Based PK Parameters: A Feasibility Study. Cancer Inform 2015;14:7-18.
- Parker GJ, Roberts C, Macdonald A, Buonaccorsi GA, Cheung S, Buckley DL, Jackson A, Watson Y, Davies K, Jayson GC. Experimentally-derived functional form for a population-averaged high-temporal-resolution arterial input function for dynamic contrast-enhanced MRI. Magn Reson Med 2006;56:993–1000.
- Orton MR, d'Arcy JA, Walker-Samuel S, Hawkes DJ, Atkinson D, Collins DJ, Leach MO. Computationally efficient vascular input function models for quantitative kinetic modelling using DCE-MRI. Phys Med Biol 2008;53:1225-39.
- 20. Zhao J, Wang YL, Li XB, Hu MS, Li ZH, Song YK, Wang JY, Tian YS, Liu DW, Yan X, Jiang L, Yang ZY, Chu JP. Comparative analysis of the diffusion kurtosis imaging and diffusion tensor imaging in grading gliomas, predicting tumour cell proliferation and IDH-1 gene mutation status. J Neurooncol 2019;141:195-203.
- Zhao J, Yang ZY, Luo BN, Yang JY, Chu JP. Quantitative Evaluation of Diffusion and Dynamic Contrast-Enhanced MR in Tumor Parenchyma and Peritumoral Area for Distinction of Brain Tumors. PLoS One 2015;10:e0138573.
- Zeng S, Ma H, Xie D, Huang Y, Wang M, Zeng W, Zhu N, Ma Z, Yang Z, Chu J, Zhao J. Quantitative susceptibility mapping evaluation of glioma. Eur Radiol 2023;33:6636-47.
- 23. Woehrer A, Sander P, Haberler C, Kern S, Maier H, Preusser M, Hartmann C, Kros JM, Hainfellner JA; Research Committee of the European Confederation of Neuropathological Societies. FISH-based detection of 1p 19q codeletion in oligodendroglial tumors: procedures and protocols for neuropathological practice a publication under the auspices of the Research Committee of the

- European Confederation of Neuropathological Societies (Euro-CNS). Clin Neuropathol 2011;30:47-55.
- 24. Tang LQ, Li CF, Li J, Chen WH, Chen QY, Yuan LX, et al. Establishment and Validation of Prognostic Nomograms for Endemic Nasopharyngeal Carcinoma. J Natl Cancer Inst 2016;108:djv291.
- 25. Song W, Wang Z, Zhang R. Classroom Digital Teaching and College Students' Academic Burnout in the Post COVID-19 Era: A Cross-Sectional Study. Int J Environ Res Public Health 2022;19:13403.
- Ulyte A, Katsaros VK, Liouta E, Stranjalis G, Boskos C, Papanikolaou N, Usinskiene J, Bisdas S. Prognostic value of preoperative dynamic contrast-enhanced MRI perfusion parameters for high-grade glioma patients.
   Neuroradiology 2016;58:1197-208.
- 27. Li SH, Shen NX, Wu D, Zhang J, Zhang JX, Jiang JJ, Zhu WZ. A Comparative Study Between Tumor Blood Vessels and Dynamic Contrast-enhanced MRI for Identifying Isocitrate Dehydrogenase Gene 1 (IDH1) Mutation Status in Glioma. Curr Med Sci 2022;42:650-7.
- 28. Ahn SH, Ahn SS, Park YW, Park CJ, Lee SK. Association of dynamic susceptibility contrast- and dynamic contrast-enhanced magnetic resonance imaging parameters with molecular marker status in lower-grade gliomas: A retrospective study. Neuroradiol J 2023;36:49-58.
- 29. Wang J, Hu Y, Zhou X, Bao S, Chen Y, Ge M, Jia Z. A radiomics model based on DCE-MRI and DWI may improve the prediction of estimating IDH1 mutation and angiogenesis in gliomas. Eur J Radiol 2022;147:110141.
- Sakai Y, Yang C, Kihira S, Tsankova N, Khan F, Hormigo A, Lai A, Cloughesy T, Nael K. MRI Radiomic Features to Predict IDH1 Mutation Status in Gliomas: A Machine Learning Approach using Gradient Tree Boosting. Int J Mol Sci 2020;21:8004.
- 31. Zhang L, Wang R, Gao J, Tang Y, Xu X, Kan Y, Cao X, Wen Z, Liu Z, Cui S, Li Y. A novel MRI-based deep learning networks combined with attention mechanism for predicting CDKN2A/B homozygous deletion status in IDH-mutant astrocytoma. Eur Radiol 2024;34:391-9.
- 32. Gao J, Liu Z, Pan H, Cao X, Kan Y, Wen Z, Chen S, Wen M, Zhang L. Preoperative Discrimination of CDKN2A/B Homozygous Deletion Status in Isocitrate Dehydrogenase-Mutant Astrocytoma: A Deep Learning-Based Radiomics Model Using MRI. J Magn Reson Imaging 2024;59:1655-64.
- 33. Ahn SS, An C, Park YW, Han K, Chang JH, Kim SH, Lee SK, Cha S. Identification of magnetic resonance imaging features for the prediction of molecular profiles of newly

- diagnosed glioblastoma. J Neurooncol 2021;154:83-92.
- 34. Kickingereder P, Bonekamp D, Nowosielski M, Kratz A, Sill M, Burth S, Wick A, Eidel O, Schlemmer HP, Radbruch A, Debus J, Herold-Mende C, Unterberg A, Jones D, Pfister S, Wick W, von Deimling A, Bendszus M, Capper D. Radiogenomics of Glioblastoma: Machine Learning-based Classification of Molecular Characteristics by Using Multiparametric and Multiregional MR Imaging Features. Radiology 2016;281:907-18.
- 35. Calabrese E, Rudie JD, Rauschecker AM, Villanueva-Meyer JE, Clarke JL, Solomon DA, Cha S. Combining radiomics and deep convolutional neural network features from preoperative MRI for predicting clinically relevant genetic biomarkers in glioblastoma. Neurooncol Adv 2022;4:vdac060.
- Calabrese E, Villanueva-Meyer JE, Cha S. A fully automated artificial intelligence method for non-invasive, imaging-based identification of genetic alterations in glioblastomas. Sci Rep 2020;10:11852.
- 37. Mills SJ, du Plessis D, Pal P, Thompson G, Buonacorrsi G, Soh C, Parker GJ, Jackson A. Mitotic Activity in Glioblastoma Correlates with Estimated Extravascular Extracellular Space Derived from Dynamic Contrast-Enhanced MR Imaging. AJNR Am J Neuroradiol 2016;37:811-7.
- 38. Aryal MP, Nagaraja TN, Keenan KA, Bagher-Ebadian H, Panda S, Brown SL, Cabral G, Fenstermacher JD, Ewing JR. Dynamic contrast enhanced MRI parameters and tumor cellularity in a rat model of cerebral glioma at 7 T. Magn Reson Med 2014;71:2206-14.
- 39. Waqar M, Lewis D, Agushi E, Gittins M, Jackson A, Coope D. Cerebral and tumoral blood flow in adult gliomas: a systematic review of results from magnetic resonance imaging. Br J Radiol 2021;94:20201450.
- 40. Nguyen TB, Cron GO, Mercier JF, Foottit C, Torres CH, Chakraborty S, Woulfe J, Jansen GH, Caudrelier JM, Sinclair J, Hogan MJ, Thornhill RE, Cameron IG. Preoperative prognostic value of dynamic contrastenhanced MRI-derived contrast transfer coefficient and plasma volume in patients with cerebral gliomas. AJNR Am J Neuroradiol 2015;36:63-9.
- 41. Bonekamp D, Deike K, Wiestler B, Wick W, Bendszus M, Radbruch A, Heiland S. Association of overall survival in patients with newly diagnosed glioblastoma with contrastenhanced perfusion MRI: Comparison of intraindividually matched T1 and T2 (\*) -based bolus techniques. J Magn Reson Imaging 2015;42:87-96.
- 42. Lee JY, Ahn KJ, Lee YS, Jang JH, Jung SL, Kim BS.

Differentiation of grade II and III oligodendrogliomas from grade II and III astrocytomas: a histogram analysis of perfusion parameters derived from dynamic contrastenhanced (DCE) and dynamic susceptibility contrast (DSC) MRI. Acta Radiol 2018;59:723-31.

Cite this article as: Ma H, Zeng S, Huang Y, Xie D, Mazu L, Zhu N, Zhao J, Yang Z, Chu J. Predicting glioma histomolecular diagnosis and prognosis: preoperative dynamic contrast-enhanced magnetic resonance imaging insights. Quant Imaging Med Surg 2025;15(10):9855-9870. doi: 10.21037/qims-2025-36

43. Chen Z, Li N, Liu C, Yan S. Deep Convolutional Neural Network-Based Brain Magnetic Resonance Imaging Applied in Glioma Diagnosis and Tumor Region Identification. Contrast Media Mol Imaging 2022;2022:4938587.

# **Supplementary**

**Table S1** The Detailed Molecular Information of 9 Cases with Gliomas of *IDH*-wildtype, NOS

ID	sex	age	IDH	1p19q	EGFR amplification	+7/-10 cytogenetic signature	CDKN2A/B homozygously deletion	necrosis	microvascular proliferation	original histologic diagnosis	original histologic WHO grade	OS (m)	survival status
1	male	47	wild-type	non-codeletion			no deletion			diffuse astrocytomas	III	24.00	dead
2	male	50	wild-type							diffuse astrocytomas	II	92.80	alive
3	male	51	wild-type			no +7/-10				gemistocytic astrocytoma	II	-	lost to follow-up
4	female	43	wild-type	codeletion				no	no	oligodendrogliomas	II	39.10	alive
5	male	65	wild-type	non-codeletion	no amplification	no +7/-10		no		diffuse astrocytomas	II	2.40	alive
6	female	40	wild-type		no amplification	no +7/-10			not obvious	diffuse astrocytomas	II	74.60	dead
7	female	48	wild-type							anaplastic astrocytoma	III		
8	male	31	wild-type	non-codeletion			no deletion			low-grade glioma	II	31.60	dead
9	female	37	wild-type		no amplification	no +7/-10		no		oligoastrocytoma	II	72.70	alive

A blank in the table indicates that the attribute was not mentioned or not tested. The following tables show the results of the univariate statistical analysis. Initially, non-parametric univariate analysis was performed to evaluate whether any significant difference was presented in different groups. Then, for statistically significant parameters, receiver operating characteristic (ROC) curve analysis was performed to assess the discriminant capacity, describing the area under the ROC curves (AUCs), sensitivity, specificity, and cut-offs. The following additional abbreviations have been used in the following tables. Unless otherwise indicated, "\*" indicates that p < 0.05, "\*\*" indicates that p < 0.01, "\*\*" indicates that p < 0.001, "ns" indicates that p > 0.05. p1, p value of the non-parametric test (two-tailed); p2, asymptotic p value of the ROC curve; 95% CI, 95% CI of AUC; Y, optimal Youden's index. In addition, the units of DCE parameters such as Ktans and Ve throughout the following tables are shown below, not displayed in the tables: The unit of Ktrans: min -1. The unit of Kep: min-1. The unit of iAUC: mM/sec. There is no unit for the DCE parameter of Ve and iAUC. WHO, World Health Organization; OS, overall survival; NOS, not otherwise specified.

Table S2 The Partial Representative Results of Non-parametric Tests and ROC Analysis of Useful Metrics for Diagnosing LGGs and HGGs

	group (	median)								
parameter	HGG (n=61)	LGG (n=40)	p1	AUC	p2	95% CI	Υ	SE	SP	cut-off
tumor.Ktrans.min	0.010	0.000	**	0.666	**	0.571 ~ 0.749	0.357	0.557	0.800	0.010
tumor.Ktrans.max	0.530	0.330	*	0.625	*	0.494 ~ 0.745	0.321	0.721	0.600	0.360
tumor.Ktrans.mean	0.150	0.060	***	0.777	***	0.683 ~ 0.842	0.444	0.869	0.575	0.080
tumor.Ve.min	0.030	0.000	***	0.748	***	0.656 ~ 0.827	0.520	0.770	0.750	0.010
tumor.Ve.max	2.480	2.030	ns	0.607	ns	0.497 ~ 0.716	0.266	0.541	0.725	2.370
tumor.Ve.mean	0.440	0.090	***	0.805	***	0.713 ~ 0.887	0.611	0.836	0.775	0.180
tumor.Kep.max	16.300	63.340	***	0.758	***	0.638~ 0.843	0.464	0.775	0.689	30.450
tumor.Kep.mean	1.580	5.235	***	0.800	***	0.670 ~ 0.898	0.610	0.725	0.885	4.320
tumor.iAUC.min	0.000	0.000	*	0.600	ns	0.486 ~ 0.708	0.195	0.295	0.900	0.000
tumor.iAUC.max	0.660	0.170	***	0.802	***	0.708 ~ 0.871	0.529	0.754	0.775	0.360
tumor.iAUC.mean	0.240	0.025	***	0.853	***	0.763 ~ 0.920	0.602	0.902	0.700	0.080
peritumoral.iAUC.max	0.020	0.010	ns	0.609	ns	0.493 ~ 0.724	0.254	0.754	0.500	0.000
peritumoral.iAUC.mean	0.010	0.000	ns	0.591	ns	0.476 ~ 0.707	0.215	0.590	0.625	0.000

ROC, receiver operating characteristic; LGG, low-grade glioma; HGG, high-grade glioma; AUC, area under the curve; CI, confidence interval; SE, sensitivity; SP, specificity; iAUC, initial area under the curve for the first 60 seconds.

Table S3 The Partial Representative Results of Non-parametric Tests and Post Hoc Pairwise Comparisons for Diagnosing Different Grades

		grade (median)			p for WHO	p for WHO	p for WHO
parameter	WHO grade 2 (n=29)	WHO grade 3 (n=11)	WHO grade 4 (n=61)	р	grade 2 vs. WHO grade 3	grade 2 vs. WHO grade 4	grade 3 vs. WHO grade 4
tumor-Ktrans-min	0.00	0.01	0.01	**	ns	***	ns
tumor-Ktrans-mean	0.06	0.11	0.15	***	ns	***	ns
tumor-Ve-min	0.00	0.04	0.03	***	**	***	ns
tumor-Ve-mean	0.08	0.46	0.44	***	**	***	ns
tumor-Kep-max	75.01	28.58	16.30	***	**	***	ns
tumor-Kep-mean	5.89	1.69	1.58	***	***	***	ns
tumor-iAUC-min	0.00	0.00	0.00	*	*	*	ns
tumor-iAUC-max	0.15	0.43	0.66	***	*	***	ns
tumor-iAUC-mean	0.01	0.16	0.24	***	*	***	ns
peritumoral-iAUC-max	0.00	0.05	0.02	*	ns	ns	ns
peritumoral-iAUC-mean	0.00	0.03	0.01	*	ns	ns	ns

WHO, World Health Organization; iAUC, initial area under the curve for the first 60 seconds.

Table S4 The partial representative AUC, Sensitivity, and Specificity Values, and Optimal Threshold for Useful Metrics for Diagnosing WHO Grade 2 gliomas

parameter	AUC	p2	95% CI	Υ	SE	SP	cut-off
tumor-Ktrans-min	0.71	**	0.604 ~ 0.816	0.438	0.542	0.897	0
tumor-Ktrans-mean	0.789	***	0.677 ~ 0.878	0.516	0.861	0.655	0.06
tumor-Ve-min	0.813	***	0.737 ~ 0.879	0.598	0.736	0.862	0
tumor-Ve-mean	0.858	***	0.763 ~ 0.928	0.695	0.764	0.931	0.19
tumor-Kep-max	0.827	***	0.739 ~ 0.912	0.557	0.724	0.833	54.68
tumor-Kep-mean	0.872	***	0.788 ~ 0.942	0.689	0.828	0.861	4.86
tumor-iAUC-min	0.605	ns	0.491 ~ 0.720	0.209	0.278	0.931	0
tumor-iAUC-max	0.84	***	0.748 ~ 0.916	0.619	0.722	0.897	0.34
tumor-iAUC-mean	0.886	***	0.810 ~ 0.950	0.702	0.806	0.897	0.1
peritumoral-iAUC-max	0.643	*	0.523 ~ 0.744	0.239	0.722	0.517	0
peritumoral-iAUC-mean	0.64	*	0.532 ~ 0.750	0.273	0.583	0.69	0

ROC, receiver operating characteristic; AUC, area under the curve; CI, confidence interval; SE, sensitivity; SP, specificity; iAUC, initial area under the curve for the first 60 seconds.

Table S5 The Partial Representative AUC, Sensitivity, and Specificity Values, and Optimal Threshold for Useful Metrics for Diagnosing WHO grade 4 gliomas

8 8							
parameter	AUC	p2	95% CI	Υ	SE	SP	cut-off
tumor-Ktrans-min	0.666	**	0.557 ~ 0.774	0.357	0.557	0.8	0
tumor-Ktrans-mean	0.777	***	0.680 ~ 0.866	0.444	0.869	0.575	0.07
tumor-Ve-min	0.748	***	0.654 ~ 0.838	0.52	0.77	0.75	0
tumor-Ve-mean	0.805	***	0.709 ~ 0.889	0.611	0.836	0.775	0.17
tumor-Kep-max	0.758	***	0.650 ~ 0.845	0.464	0.775	0.689	27.99
tumor-Kep-mean	0.8	***	0.693 ~ 0.901	0.61	0.725	0.885	4.31
tumor-iAUC-min	0.597	ns	0.486 ~ 0.708	0.195	0.295	0.9	0
tumor-iAUC-max	0.802	***	0.701 ~ 0.888	0.529	0.754	0.775	0.34
tumor-iAUC-mean	0.853	***	0.768 ~ 0.925	0.602	0.902	0.7	0.07
peritumoral-iAUC-max	0.61	ns	0.496 ~ 0.714	0.254	0.754	0.5	0
peritumoral-iAUC-mean	0.591	ns	0.484 ~ 0.701	0.215	0.59	0.625	0

ROC, receiver operating characteristic; LGG, low-grade glioma; HGG, high-grade glioma; AUC, area under the curve; CI, confidence interval; SE, sensitivity; SP, specificity; iAUC, initial area under the curve for the first 60 seconds.

Table S6 The Partial Representative Results of Non-parametric tests and ROC Analysis of Useful Metrics for Diagnosing the Genotype of IDH

	IDH (m	nedian)								
parameter	wild-type (n=61)	mutation (n=36)	p1	AUC	p2	95% CI	Υ	SE	SP	cut-off
tumor-Ktrans-min	0.010	0.000	*	0.629	*	0.540 ~ 0.714	0.272	0.516	0.757	0.000
tumor-Ktrans-mean	0.150	0.080	***	0.713	***	0.584 ~ 0.802	0.358	0.547	0.811	0.130
tumor-Ve-min	0.030	0.000	***	0.710	***	0.613 ~ 0.819	0.421	0.719	0.703	0.000
tumor-Ve-mean	0.420	0.090	***	0.738	***	0.643 ~ 0.828	0.467	0.656	0.811	0.340
tumor-Kep-max	21.630	54.680	***	0.705	***	0.559 ~ 0.815	0.370	0.730	0.641	27.990
tumor-Kep-mean	1.720	5.160	***	0.714	***	0.606 ~ 0.820	0.473	0.676	0.797	3.970
tumor-iAUC-max	0.590	0.240	***	0.710	***	0.601 ~ 0.788	0.476	0.719	0.757	0.340
tumor-iAUC-mean	0.220	0.050	***	0.770	***	0.690 ~ 0.868	0.459	0.594	0.865	0.170

ROC, receiver operating characteristicAUC, area under the curve; CI, confidence interval; SE, sensitivity; SP, specificity; iAUC, initial area under the curve for the first 60 seconds.

 $\textbf{Table S7} \ \ \text{The Partial Representative Results of Non-parametric Tests and ROC Analysis of Useful Metrics for Diagnosing the Genotype of 1p19q$ 

	1p19q (median)									
parameter	codeletion (n=19)	non-codeletion (n=66)	p1	AUC	p2	95% CI	Υ	SE	SP	cut-off
tumor-Ktrans-min	0.000	0.000	*	0.657	*	0.535 ~ 0.757	0.327	0.485	0.842	0.000
tumor-Ve-min	0.000	0.020	**	0.702	**	0.574 ~ 0.811	0.411	0.621	0.789	0.000
tumor-Ve-mean	0.110	0.375	*	0.687	*	0.541 ~ 0.837	0.388	0.652	0.737	0.160
tumor-Kep-max	70.650	27.510	**	0.705	**	0.575 ~ 0.828	0.388	0.737	0.652	42.040
tumor-Kep-mean	5.190	1.895	**	0.708	**	0.563 ~ 0.835	0.389	0.632	0.758	5.150
tumor-iAUC-mean	0.030	0.150	*	0.677	*	0.533 ~ 0.802	0.359	0.727	0.632	0.070

ROC, receiver operating characteristic; AUC, area under the curve; CI, confidence interval; SE, sensitivity; SP, specificity; iAUC, initial area under the curve for the first 60 seconds.

Table S8 The Partial Representative Results of Non-parametric Tests and ROC Analysis of Useful Metrics for Diagnosing the Genotype of CDKN2A/B Homozygous Deletion

parameter	CDKN2A/B ho	4	o1 AUC		050/ 01		0.5	0.0		
	no deletion (n=43)	deletion (n=5)	p1	AUC	p2	95% CI	Y	SE	SP	cut-off
tumor-Ve-max	2.060	2.960	**	0.930	**	0.857 ~ 1.004	0.907	1.000	0.907	2.870
tumor-Ve-mean	0.090	0.700	*	0.830	*	0.719 ~ 0.942	0.744	1.000	0.744	0.190
tumor-Kep-min	0.030	0.000	*	0.784	*	0.645 ~ 0.922	0.674	0.674	1.000	0.010
tumor-Kep-mean	5.190	1.580	*	0.837	*	0.701 ~ 0.974	0.674	0.674	1.000	4.000
tumor-iAUC-max	0.220	0.440	*	0.777	*	0.597 ~ 0.956	0.581	1.000	0.581	0.240
tumor-iAUC-mean	0.030	0.140	*	0.791	*	0.644 ~ 0.937	0.628	1.000	0.628	0.070

ROC, receiver operating characteristic; AUC, area under the curve; CI, confidence interval; SE, sensitivity; SP, specificity; iAUC, initial area under the curve for the first 60 seconds.

Table S9 The Partial Representative Results of Non-parametric tests and ROC Analysis of Useful Metrics for Diagnosing the Genotype of EGFR

	EGFR amplific	ation (median)				<u> </u>				
	no amplification (n=37)	amplification (n=19)	p1	AUC	p2	95% CI	Υ	SE	SP	cut-off
tumor-Ve-min	0.020	0.050	ns	0.649	ns	0.505 ~ 0.793	0.326	0.947	0.378	0.000
peritumoral-Ve-mir	0.020	0.010	ns	0.649	ns	0.502 ~ 0.797	0.331	0.595	0.737	0.010
tumor-iAUC-mean	0.190	0.270	ns	0.648	ns	0.499 ~ 0.797	0.280	0.632	0.649	0.250

ROC, receiver operating characteristic; AUC, area under the curve; CI, confidence interval; SE, sensitivity; SP, specificity; iAUC, initial area under the curve for the first 60 seconds.

**Table S10** The Partial Representative Results of Non-parametric Tests and ROC Analysis of Useful Metrics for Diagnosing the Genotype of +7/–10 Cytogenetic Signature

	+7/-10 cyt	•		AUC	p2	050/ 01	Υ		SP	cut-off
	no +7/-10 (n=18)	+7/-10 (n=2)	- p1			95% CI		SE		
peritumoral-Ktrans-max	0.090	0.035	ns	0.903	ns	0.728 ~ 1.078	0.778	0.778	1.000	0.050
peritumoral-Ve-max	0.210	0.020	ns	0.903	ns	0.758 ~ 1.048	0.778	0.778	1.000	0.030
peritumoral-Ve-mean	0.075	0.010	ns	0.917	ns	0.779 ~ 1.054	0.833	0.833	1.000	0.020

ROC, receiver operating characteristic; AUC, area under the curve; CI, confidence interval; SE, sensitivity; SP, specificity; iAUC, initial area under the curve for the first 60 seconds.

**Table S11** The Partial Representative Results of Logistic Models for Predicting HGG, WHO Grade 2, WHO Grade 4, *IDH* Mutation, 1p19q Codeletion, and *CDKN2A/B* Homozygous Deletion

model	N	AUC	SE	SP	Υ	cut-off	accuracy	PPV	NPV
pro-group	101	0.870	0.82	0.8	0.62	0.608	0.811	0.836	0.70
pro-grade2	101	0.893	0.793	0.903	0.696	0.494	0.861	0.759	0.903
pro-grade4	101	0.858	0.82	0.8	0.62	0.54	0.802	0.86	0.727
pro-IDH	101	0.85	0.892	0.703	0.595	0.264	0.762	0.627	0.9
pro-1p19q	85	0.705	0.652	0.737	0.388	0.798	0.659	0.894	0.368
pro-CDKN2A/B	48	0.93	1	0.907	0.907	0.315	0.896	0.5	0.975

AUC, area under the curve; CI, confidence interval; SE, sensitivity; SP, specificity; PPV, positive predictive value; NPV, negative predictive value.